Biochimica et Biophysica Acta 1848 (2015) 41–50

Contents lists available at ScienceDirect

Biochimica et Biophysica Acta

journal homepage: www.elsevier.com/locate/bbamem

Stalk formation as a function of lipid composition studied by X-ray reflectivity

Ziad Khattari [a], Sebastian Köhler [b], Yihui Xu [b], Sebastian Aeffner [b], Tim Salditt [b,*]

[a] Department of Physics, Hashemite University, 13115 Zarqa, Jordan
[b] Institut für Röntgenphysik, Universität Göttingen, Friedrich-Hund-Platz 1, 37077 Göttingen, Germany

ARTICLE INFO

Article history:
Received 11 April 2014
Received in revised form 24 July 2014
Accepted 8 August 2014
Available online 28 September 2014

Keywords:
Membrane fusion
Stalk structure
Multi-component lipid bilayer
X-ray reflectivity

ABSTRACT

We have investigated the structure and interaction of solid-supported multilamellar phospholipid bilayers in view of stalk formation as model systems for membrane fusion. The multi-component bilayers were composed of ternary and quaternary mixtures, containing phosphatidylcholines, phosphatidylethanolamines, sphingomyelin, cholesterol, diacylglycerol, and phosphatidylinositol. Analysis of the obtained electron density profiles and the pressure–distance curves reveals systematic changes in structure and hydration repulsion. The osmotic pressure needed to induce stalk formation at the transition from the fluid lamellar to the rhombohedral phase indicates how membrane fusion properties are modified by bilayer composition.

1. Introduction

Membrane fusion is a ubiquitous biological process, from membrane trafficking and exocytosis to viral infection and synaptic transmission [54,19,44,17,20]. Membranes do not fuse spontaneously, but in a highly orchestrated and controlled process, overcoming the energy barrier which normally prevents unspecific fusion to sustain the compartmentalized structure of cells. Energy must be supplied to overcome the hydration repulsion between two membranes, i.e.to remove water molecules from the cleft between them and to achieve the highly curved state of the lipid monolayers, enabling the topological transformation. In biological membrane fusion, this energy is provided by highly specialized fusion proteins [22]. However, depending on lipid composition, membrane fusion can also occur in pure lipidic membranes by imposing external forces [8,16], for example by osmotic stress [27]. For this protein-free fusion of lipid bilayers, Kozlov and Chernomordik have proposed a generic pathway based on a number of intermediate states and have worked out the basic mechanical description [26,11,49,50,9], see also [10] for a review. The link to biological fusion is then developed on the idea that fusion proteins exert forces which bring the opposing membrane in close juxtaposition and also create membrane stresses which in turn drive the fusion of lipid bilayers. An important intermediate structure is considered to be the fusion stalk, a neck-like connection between fusing membranes, which is regarded as the first high energy intermediate state along the fusion pathway. Many experimental and theoretical studies have consolidated the stalk hypothesis and the existence of several intermediates on the pathway to membrane fusion [21,20]. After significant method development, molecular dynamics (MD) simulation can now also quantify the Gibbs free energy difference between separated bilayers and a stalk, as well as the subsequent energy barriers (hemifusion diaphragm, fusion pore) [24].

X-ray and neutron diffraction have since long been employed in the study of model lipid membranes, yielding high-resolution (down to Å scale) structural details [18,39,51,23,40]. Recently, we have provided a high resolution X-ray analysis of the stalk structure in several different lipid membrane systems [3], using the approach of equilibrium stalk phases, as introduced by the seminal work of Yang and Huang [59]. In this model system, stalk formation in multilamellar membranes is induced by dehydration, replacing the constraints imposed in the biological context by fusion proteins with osmotic pressure as an external control parameter. Accordingly, the three-dimensional (3D) continuum electron density of the stalk can be determined, as well as the pressure distance curves characterizing the transition from the fluid lamellar phase (denoted in the following as L-phase) to the stalk phase, which exhibits rhombohedral symmetry (denoted in the following as the R-phase), reflecting the global symmetry formed by the long range order of the stalks in the multilamellar 'host'. While the stalk structure was found to be 'highly conserved', if scaled to the lipid bilayer thickness, the energetics was found to vary significantly depending on the lipid composition, for all seven lipid systems studied, which comprised both single component as well as two component mixtures. In this work we extend the previous X-ray study of single component and two-component lipid model systems, to multi-component lipid mixtures composed of three or four lipid constituents, see also the overview in Fig. 1. The goal of the work is to screen a higher number of mixtures in

* Corresponding author.
E-mail addresses: zkhattari@hu.edu.jo (Z. Khattari), tsalditt@gwdg.de (T. Salditt).

http://dx.doi.org/10.1016/j.bbamem.2014.08.010
0005-2736/

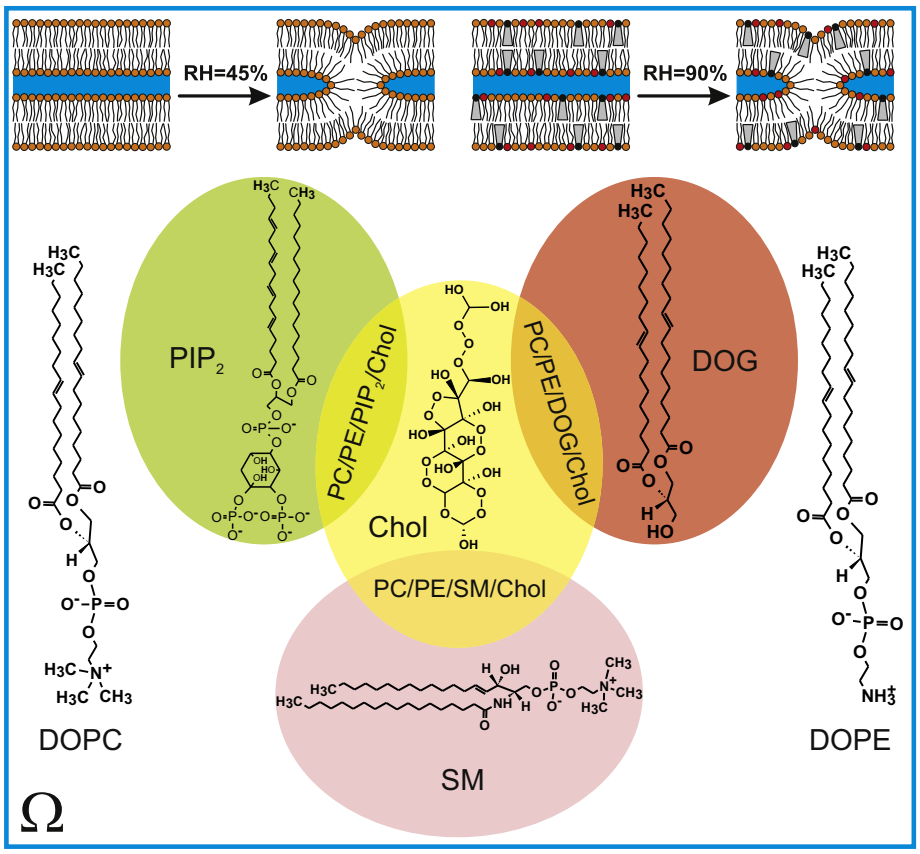

Fig. 1. Venn diagram illustration of the lipids used in this study. Ω represents the total set of all lipids as shown in the figure. Each sub-group is represented by an ellipse. The intersections of the sub-groups are the phospholipid mixtures investigated experimentally. The DOPC/DOPE mixture is present in every sample.

view of their respective propensity to form stalks, using laboratory X-ray instrumentation only, for reasons of long term accessibility. Since the full 3D structure analysis necessitates the use of synchrotron radiation, at least at the high resolution presented in [3], we here content ourselves with determining the transition point from the L-phase to the R-phase, i.e. the critical relative humidity RH^* (or osmotic pressure, correspondingly), at which stalk formation occurs in a given mixture. In addition we determine the corresponding dehydration energy from the osmotic pressure. To this end, we make use of the inhouse X-ray reflectometer setup and the procedures already described in [2,3], see also the schematic of Fig. 2. We thus compare various lipid mixtures containing biologically significant components, mainly by approaching the L-to-R transition from the low osmotic pressure side, i.e. from the L-phase. In this way, we can quantify how the hydration force between membranes and the transition point are affected by the composition. While the high osmotic pressure phase has been identified as the R-phase for some of the mixtures by two-dimensional diffraction in our previous work, we cannot be certain for all lipid mixtures studied in this work that this phase is in fact the R-phase and not another non-lamellar phase. However, we consider this to be extremely unlikely based on the signature of the transition itself. As detailed in the manuscript, the signature of the transition to the R-phase as probed by reflectivity (momentum transfer perpendicular to the membrane, i.e. along q_z) follows a characteristic pattern for the L–R transition.

In the following, we briefly summarize the assumed roles of different lipids in membrane fusion. Membrane fusion is known to be affected by the lipid composition, even though the exact local composition at the fusion site is not precisely known, and can be expected to deviate from the average as for other functional sites [52]. For each lipid species, the spontaneous curvature is a major factor [6]. Cone shaped lipids of positive spontaneous curvature such as phosphatidylcholines (PC) are considered to inhibit stalk formation and fusion, and lipids of negative spontaneous curvature (inverse cone shaped) such as phosphatidylethanolamines (PE) are considered to favor stalk formation and to promote fusion. PC as one of the major lipid species in mammalian membranes, has strongly hydrated headgroups and forms stable bilayers [56], which fuse only at very high osmotic pressure. PE as another major component of mammalian membranes, has a cone-shaped molecular structure and the ability to promote non-lamellar phases with negative curvature, such as the inverse hexagonal phase. Sphingomyelin (SM) with molecular shape and hydration properties similar to PC is involved in raft formation in the presence of cholesterol (Chol) [28,57,33].

The change of the phase transition point with PC/PE molar ratio is remarkable. Starting with the single component systems, the L → R phase transition occurs at $RH^* \approx 46\%$ for 1,2-dioleoyl-*sn*-glycero-3-phosphatidylcholine (DOPC) ($T = 20$ °C), whereas pure 1,2-dioleoyl-*sn*-glycero-3-phosphatidylethanolamine (DOPE) forms the inverse hexagonal phase instead of the R-phase [58,3]. Phase diagrams of DOPC/DOPE, however, show a stable R-phase over a large range of compositions and up to significantly higher *RH* values than pure DOPC. For DOPC/DOPE:75/25 ratio, Yang et al. have already shown that the L → R phase transition occurs at $RH^* \approx 66\%$ [58]. It was also found that increasing temperature is equivalent to increasing DOPE in the mixture, and decreasing temperature is equivalent to increasing DOPC in the mixture. The phase diagram at constant temperature as a function of molar ratio was given in [2,3].

Chol, which is present in most mammalian membranes, but in very different amounts depending on the organelle [41], enhances bilayer fluidity, reduces the passive permeability, and increases the mechanical strength and bending rigidity κ [37]. At the same time Chol also leads to a more negative intrinsic curvature [6], which can point to an important role in fusion [12]. For DOPC and 1,2-diphytanoyl-*sn*-glycero-3-phosphatidylcholine (DPhPC) moderate addition of Chol was found to strongly promote the R-phase. In the case of DOPC, the R-phase forms at

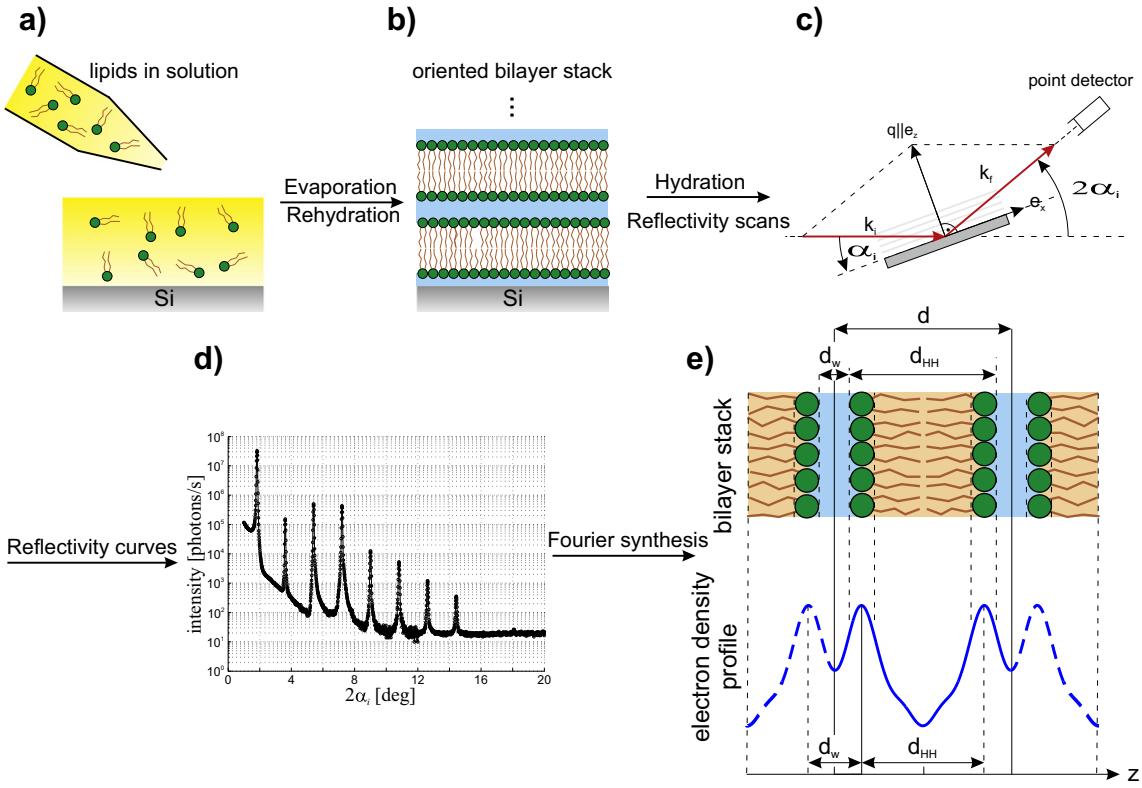

Fig. 2. The method and steps used in our experiment: (a) and (b) sample preparation of highly aligned phospholipid bilayers, (c) the reflectivity geometry, (d) typical reflectivity curves and finally (e) the resulting electron density profile.
Adapted from [1].

RH < 65% at a cholesterol concentration of 30 mol%. In DPhPC/Chol, the R phase was observed at cholesterol concentration up to 15% where a pure R phase was found at *RH* < 87% [2]. Moderate concentration of Chol in DOPC or Chol in DPhPC also promotes the R-phase [3].

Another important group of phospholipids which is involved in signal transduction is the phosphoinositide [38]. In spite of their low abundance in cell membrane (less than 10% of cell membrane), the phosphoinositides are of enormous physiological importance. They are found exclusively on the inner leaflet of the plasma membrane. Due to their negative charge they can alter the membranes' physical properties, such as local charge density and local curvature when mixed with other phospholipids [35]. In particular, phosphatidylinositol 4,5-bisphosphate (PIP_2) is an important lipid in the regulation of several cellular processes including membrane fusion. According to molecular dynamics (MD) simulations, PIP_2 changes the structural properties of the host lipid bilayer by rearranging and reorganizing its surrounding lipids to form stable microdomains [31]. The phase diagram of PC/PIP_2 shows that it can promote non-lamellar phases [14]. At low concentration, PIP_2 promotes the stalk-phase, and at higher concentration the formation of the hexagonal phase, which is usually not observed for pure DOPC.

Finally, it is well known that small molar fractions (less than 2 mol%) diacylglycerol (DAG) can induce thermotropic lamellar to non-lamellar phase transition, for example in PC/Chol or SM-containing bilayers [48,4], and that physiological levels of DAG can substantially increase the fusion propensity of phospholipid membranes [51]. Note that many reported studies have used more complex lipid compositions to model membrane fusion [16,4], but not necessarily in combination with the structural techniques. A large variety of lipid compositions were tested in vesicle based optical experiments, for example with regard to their ability to promote hemifusion, fusion and vesicle rupture. The lipid composition with highest fusion efficiency without content leakage was a mixture of PC:PE:SM:Chol (35:30:15:20) [16]. Interestingly, this composition is close to the lipid composition of synaptic vesicles, except for the lack of phosphatidylserine (PS). The negatively charged PS inhibits the fusion of pure lipid vesicles. The presence of PE in lipid bilayer promotes fusion, whereas the SM:Chol components at appropriate ratios reduce vesicle rupture upon osmotic compression and facilitates membrane fusion.

The present study is designed as follows: as majority lipids we use phosphatidylcholine (PC) and phosphatidylethanolamine (PE), where RH^* can be shifted to higher values by increasing the PE:PC ratio [2,3]. Concerning chain length and saturation, 1,2-dioleoyl chains were chosen in view of fluidity, bilayer thickness, literature reference data and phase state at room temperature, where all measurements have been performed. Note that lipids with saturated chains do not form the R-phase (stalk phase) at low hydration, but favor gel phases and tightly packed chains. Into these 'host' lipids we mix small amounts of 'additive' lipids, notably Chol, PIP_2, and DAG. Chol was previously shown to promote the stalk phase in pure DOPC [2] in agreement with [59,60]. PIP_2, which enhances the interaction of synaptic vesicles with a phosphatidylcholine lipid monolayer at the air/water interface [15], was also shown to promote the stalk phase in PC, as well as the hexagonal phase at higher concentration [14]. We investigate how the critical value RH^* of the phase transition between the L-phase and the R-phase shifts, i.e. how strongly stalk formation is promoted. In particular, we study whether the effects of two stalk promoting lipids are additive, i.e. whether stalk formation can be shifted to mild dehydration (osmotic stress) by the combined effects. A major motivation of this work is to find a mixture, where stalk formation can be studied in excess solvent instead of a humidity chamber. To this end, we also include a 'magic' fusogenic mixture reported in literature in this structural study.

The paper is organized as follows: After this introduction, Section 2 presents the details on sample preparation. The data analysis is presented in Section 3. The reflectivity results obtained at varied *RH* levels and different lipid compositions, and the corresponding electron density profiles (EDP), structural and interaction parameters are presented in

Section 4. The paper closes with a discussion and conclusions in Section 5.

2. Materials and methods

The lipids 1,2-dioleoyl-*sn*-glycero-3-phosphatidylcholine (DOPC), 1,2-dioleoyl-*sn*-glycero-3-phosphatidylethanolamine (DOPE), phosphatidylinositol-4,5-bisphosphate (PIP_2, from porcine brain, NH_4^+ counterions), 1-2-dioleoyl-*sn*-glycerol (DOG) and porcine brain sphingomyelin were purchased as lyophilized powders from Avanti Polar Lipids (Alabaster, AL, USA). Cholesterol (Chol) was purchased from Sigma (St. Louis, MO, USA). All components had a purity of >99% and were used without further purification. Fig. 1 shows the molecular structure of the lipids used in this study. Solid supported stacks of typically about 10^3 aligned phospholipid bilayers of different binary and ternary mixtures were prepared by spreading from solution [29], see Fig. 2. Mixtures containing cholesterol were prepared from stock solutions ($c = 10$ mg/ml) by dissolving the lipids and cholesterol in chloroform/(2,2,2)-trifluoroethanol (1:1 vol/vol), while mixtures containing PIP_2 were prepared from stock solutions ($c = 10$ mg/ml) by dissolving the lipids and PIP_2 in a 20:9:1 (vol/vol/vol) mixture of chloroform, methanol and water respectively [15]. Polished silicon wafers with ⟨100⟩ orientation (Silchem, Freiberg, Germany) were cut into 25×15 mm^2 and were thoroughly cleaned by subsequent sonication in methanol and ultrapure water. The Si-substrate surface was rendered hydrophilic in a plasma cleaner (Harrick PDC-002). 150 μl of lipid solution was pipetted onto each substrate. After evaporation of the bulk solvent, samples were stored in vacuum overnight to extract the remaining solvent. Where necessary to achieve hydrated and equilibrated fluid phases, samples were heated prior to the measurements to $T =$ 40–50 °C for few hours in a saturated water vapor atmosphere and cooled down to 20 °C, at which all measurements were performed. Subsequently, samples were stored in a humid atmosphere for several hours. We stress that by the nature of the preparation, the lipid distribution in the two monolayers is always symmetric.

3. Data collection and analysis

The samples were placed vertically in a closed chamber with Kapton windows and re-hydrated from water vapor using a setup for relative humidity (*RH*) control described in [2,3]. As well known, *RH* can be used as a control parameter to impose an osmotic pressure Π on the bilayer stack [42], according to

$$\Pi = -\frac{k_B T}{v_w} \ln\left(\frac{RH}{100\%}\right), \tag{1}$$

where k_B denotes Boltzmann's constant, T the absolute temperature and $v_w \approx 30$ Å^3 is the volume occupied by one water molecule. The temperature was maintained at 20 °C by a fluid flow connected to a temperature-controlled reservoir (Julabo).

At small inter-bilayer separations, the osmotic pressure is balanced by the hydration repulsion $\Pi(d_w)$, which is empirically written as an exponentially decaying function of water layer thickness d_w

$$\Pi(d_w) = P_0 \exp\left(\frac{-d_w}{\lambda_h}\right), \tag{2}$$

with a characteristic decay length λ_h and a pre-exponential factor P_0.

The procedure for X-ray reflectivity measurements and analysis followed closely those described in detail in [3,1]. In brief, the chamber was placed on a home-built reflectometer equipped with a Huber goniometer stage and a sealed tube (Seifert, line focus) generating Cu-K_α radiation ($\lambda = 1.541$ Å), see Fig. 2. The X-ray beam was parallelized and monochromatized by a Göbel mirror system and collimated to a size of 0.5×5 mm^2 by a set of motorized slits, yielding a primary intensity of $4.8 \cdot 10^8$ photons per second. X-ray reflectivity (XR) curves were recorded as a function of the angle of incidence α_i, from 0 to 10° with a step size of 0.01° and 2 s exposure per data point using a fast scintillation counter (Cyberstar, Oxford-Danfysik) and automated attenuators. Reflectivity scans were repeated at different hydration levels ($35\% \le RH \le 94\%$) as shown in Figs. 3 and 4, and thus different lamellar repeat spacings d in order to apply the swelling method for phase determination [25]. After illumination correction and subtraction of the diffuse background measured by offset scans, the curves are plotted as a function of momentum transfer $q_z = \frac{4\pi}{\lambda} \sin\alpha_i$ perpendicular to the substrate surface (i.e. parallel to the bilayer normal). The lamellar repeat spacing d_{RH} for each hydration level is readily obtained from the Bragg peak positions $q_z = q_{n,RH}$ using $d_{RH} = n \cdot 2\pi/q_{n,RH}$. The integrated intensity $I_{n,RH}$ (i.e. the area under the n^{th} Bragg peak) yields the corresponding form factor amplitude $|F_{n,RH}| = \sqrt{n \cdot I_{n,RH}}$, where the factor n is the low-angle approximation of the Lorentz correction factor for oriented lipid multilayers [33].

Due to the mirror plane symmetry of lamellar phases, the form factors are real and thus restricted to $\nu_n|F_{n,RH}|$ where $\nu_n = \pm 1$. The phase factors ν_n are determined by the swelling method. To this end, one makes the assumption that small changes in hydration primarily affect the thickness of the water layer between adjacent bilayers, but leave the bilayer structure itself approximately constant. In particular, this approximation can be made for each *RH* in a differential manner, i.e. the reflectivity curves of the adjacent *RH* can be used. It can then be shown that the discrete data points $\{\nu_n|F_{n,RH}|\}$ should coincide with the continuous form factor $F(q_z)$ reconstructed from the phased $\{F_{n,RH}\}$ at one hydration level by

$$F(q_z) = \sum_n \nu_n |F_{n,RH}| \frac{\sin\left[\frac{d_{RH}}{2}\left(q_z - q_{n,RH}\right)\right]}{\frac{d_{RH}}{2}\left(q_z - q_{n,RH}\right)}. \tag{3}$$

The $\{|F_{n,RH}|\}$ for one sample at different hydration levels is normalized by the condition $(2\pi/d_{RH}) \sum_n |F_{n,RH}|^2 = \text{const}$. [5]. The form factor of order zero, F_0, is not directly accessible, as the corresponding reflection coincides with the primary beam. However, it can be approximated by

$$F_{0,RH} = 2\sum_{n>0} (-1)^{n+1} \nu_n |F_{n,RH}|, \tag{4}$$

as derived in [55]. Out of all 2^n possible phase combinations $\{\nu_n\}$, the one for which the continuous form factor $F(q_z)$ and the discrete data points $\{\nu_n|F_{n,RH}|\}$ match best (minimum residual sum of squares) is considered the most reasonable one. For some orders of diffraction, sign changes were incorporated to obtain the best fit. A typical form factor plot is shown in Fig. 4. Using the obtained form factor amplitudes and phases, the electron density profiles $\rho(z, RH)$ in arbitrary units are constructed by Fourier synthesis (for more details see [3,1])

$$\rho(z, RH) = \sum_n \nu_n |F_{n,RH}| \cos\left(q_{n,RH} \cdot z\right). \tag{5}$$

Importantly, as a result we obtain $\rho(z, RH)$ for each *RH*, and are thus able to inspect changes in the bilayer structure with dehydration. This is also important in view of deriving the parameters of the hydration repulsion, P_0 and λ_h, since these parameters are derived from plotting the osmotic pressure against water layer thickness d_w, according to Eq. (2). To this end d_w has to be determined from $\rho(z, RH)$ for each data point without the assumption of a constant bilayer structure.

Due to space constraints, it is impossible to plot all measured reflectivity curves, nor the respective $\rho(z)$. We therefore give just selected examples to illustrate the data reduction, while a larger set of XR curves and density profiles are shown in the Supplementary Material, Fig. S1 and S2, respectively. Fig. 3a shows a representative set of XR curves of

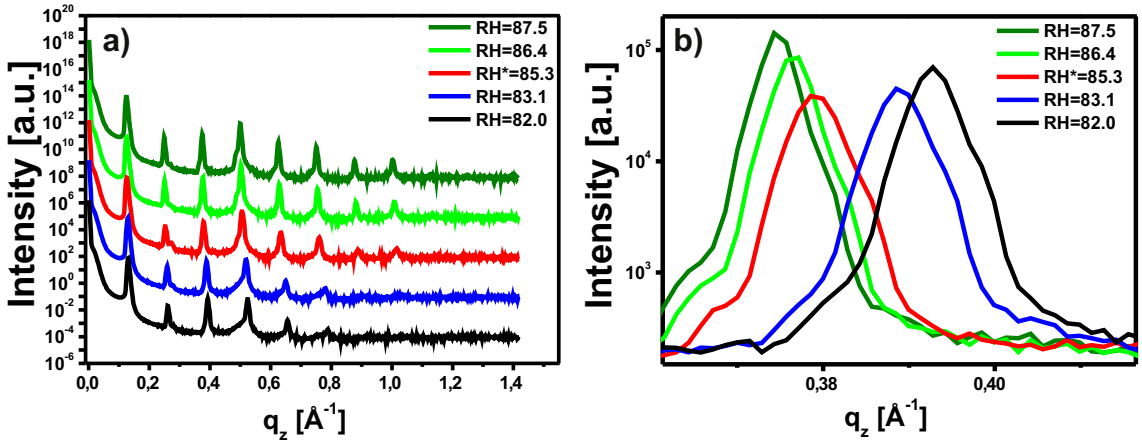

Fig. 3. Representative set of XR curves as a function of the momentum transfer from (a) DOPC/DOPE/Chol: 35/35/30 mol% bilayer stacks at various *RH* below and above the transition RH^* level. The curves are shifted vertically for clarity. The reflectivity data shows eight clearly resolved orders of diffraction. (b) The panel represents the third Bragg peak at which the transition from the lamellar (L) to rhombohedral (R) phase appears. The transition RH^* level curve is colored red. The temperature was kept constant inside the humidity chamber at $T = 20$ °C.

a DOPC/DOPE/Chol: 35/35/30 mol% sample at different hydration levels. A particularly important point is the identification of the phase transition RH^*. From comparison of reflectivity and previous GISAXS measurements, we know that the phase transition from the lamellar to the stalk (rhombohedral) phase is accompanied by a characteristic minimum of the 3rd or 4th Bragg peak, as illustrated in Fig. 3. The measured intensity is plotted as a function of the reciprocal space coordinate q_z and shifted vertically for clarity, for (a) the full q range and (b) a zoom corresponding to the relevant 3rd Bragg peak. Both from previous measurements at different synchrotron beamlines, as well as using a two-dimensional pixel detector (Pilatus, Dectris) on the same inhouse setup, we know that the dip in the 3rd Bragg peak's reflectivity occurs simultaneously with the emergence of the stalk satellite reflections, see Supplementary Material, Fig. S4. Therefore this feature has been selected as a criterion for the transition.

Supplementary Material, Fig. S1 shows the full set of samples of different molar fractions for selected hydration levels, from which the variation of RH^* with sample composition can be directly inferred. For example at DOPC/DOPE: 45:45 and 10 mol% Chol or PIP_2 concentration, the RH^* level is 87.5% or 79.8%, respectively. The different sample systems exhibit various hydration levels, but all of them preserve the general behavior of solid supported multilayer stacks. The high orientation of the multi-lamellar stacks is evidenced by a single series of sharp, equidistant Bragg peaks indicating a single lattice constant, also for the

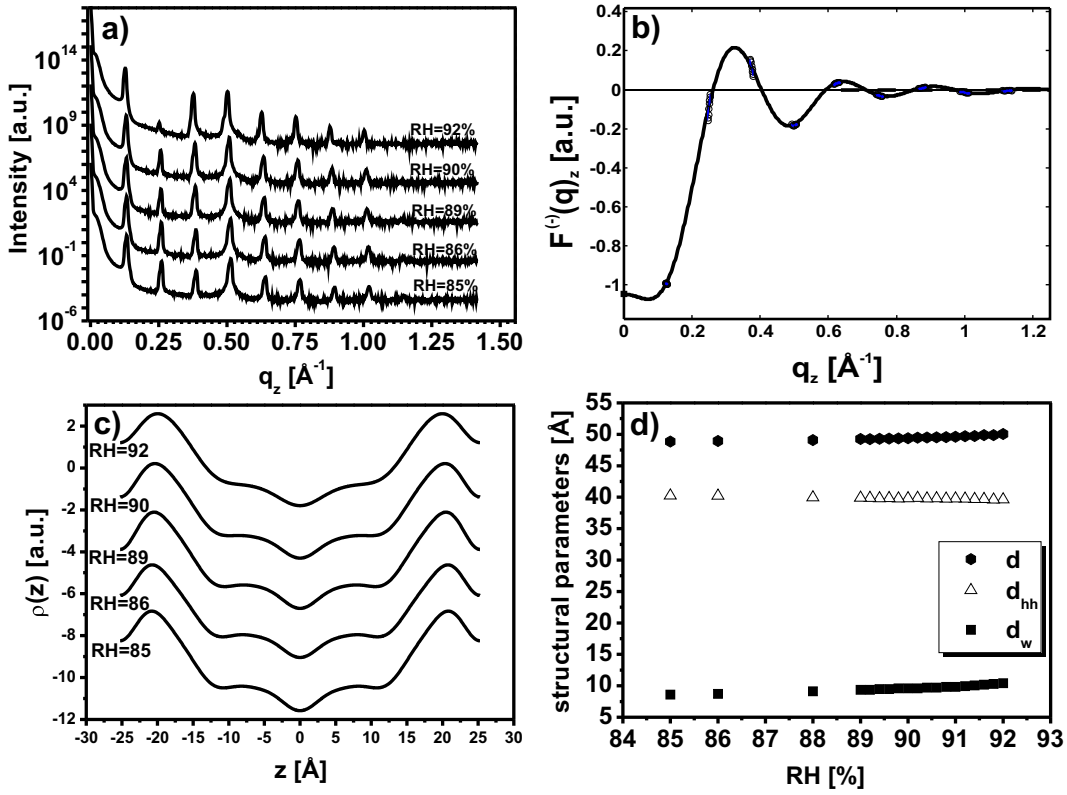

Fig. 4. Bilayer structure as determined from the EDPs: (a) Exemplary plot of the reflectivity curves deep in the lamellar phase for a DOPC/DOPE/PIP_2: 45/45/10 mol% sample at different *RH* values. The curves are shifted vertically for clarity. (b) Typical plots illustrating the swelling method for phase determination for calculating the EDPs. (c) Corresponding electron density profiles $\rho(z)$ as deduced by the swelling method. (d) Structural parameters as a function of *RH* above the transition level RH^*.

ternary mixtures DOPC/DOPE/Chol and DOPC/DOPE/PIP_2. Within the experimental resolution presented, the peak width was the same in all peak orders. For high hydration levels (i.e., $\Pi \rightarrow$ zero), the increasing distance between bilayers weakens the forces between them which results in an increase in the undulation fluctuations of the bilayers. The consequence is damping of the higher order Bragg peaks and broadening of the remaining ones [45]. All the samples were recorded over a broad range of *RH* intervals covering both L and R phases in order to identify RH^*. As discussed above, Fig. 3b shows the third Bragg peak where the transition from L to R phase appears at $RH^* = 85.3\%$. The transition hydration is associated with a reduction in the peak intensity compared with the surrounding peaks (see Supplementary Material, Fig. S1). Similar behavior is observed for all other samples. Contrarily, in the case of phase-separated domains in a mixed lipid system, one would expect two or more coexisting lattice spacings. With increasing Chol or PIP_2 content, the Bragg peaks shift towards lower q_z value, while the intensities of the higher diffraction orders are reduced. In most samples eight diffraction orders have been used for further analysis of $\rho(z)$.

Fig. 4 exemplifies the work flow from the measured XR curves to the structural bilayer parameters, in this case for DOPC/DOPE/PIP_2: 45/45/10 mol%. Fig. 4a shows typical XR curves of this ternary mixture at high *RH* levels deep in the L-phase. A typical form factor plot obtained by the swelling method for determination of the phase factors $\nu_n = \pm 1$ is shown in Fig. 4b. The corresponding EDPs for each *RH* level are shown in Fig. 4c. Maxima correspond to the mean position of the lipid head-group regions with relatively high electron density, whereas the minimum at $z = 0$ indicates the region of acyl–acyl content of the opposing hydrocarbon chains in the bilayer interior. The two local minima at $z = \pm d/2$ next to the head-group maxima represent the interbilayer water region. Fig. 4c shows a monotonous increase in the lattice spacing *d* with increasing *RH* value, which is accompanied by a broadening of the head-group peaks and a decrease in the distance between head-group regions and water layers. The lipid mixtures' bilayer structural parameters as a function of *RH* are presented in Fig. 4d.

They were extracted from the EDPs as follows: The head-group distance d_{HH} directly deduced from the EDPs is used as a measure for the bilayer thickness. Therefore, we define the corresponding water layer thickness as $d_w = d - d_{HH}$. In doing so, we are able to further analyze the effect of *RH* and Chol or PIP_2 addition on the a structural parameters (for more information see Supplementary Material, Figs. S2 & S3). All scattering form factors are consistent with fluid phase bilayers and show only small variations with changing *RH*. For DOPC/DOPE/PIP_2 presented here, *d* decreases from 50.1 Å at high $RH = 92\%$ to 48.6 Å at the transition value $RH^* = 82\%$. For the water layer distance at the transition we find $d_w^* \simeq 9 \pm 0.5$ Å, as evidenced in Fig. 4d. In fact, in all measured systems this value d_w^* appears to be universal, regardless of lipid composition or ratio [3].

4. Results

The results of this work are formed by three different but interrelated pieces of information which are presented here in the following sequence: (i) the electron density profiles (EDPs) of the different mixtures in the lamellar phase and the associated structural changes, (ii) the hydration interaction of the different mixtures on the pathway to the phase transition (dehydration), and finally (iii) the transition point RH^* itself.

Fig. 5 presents a visualization of the dehydration process for selected EDPs for single (i.e., DOPC), binary (DOPC/DOPE) and ternary (DOPC/DOPE/Chol) systems in the L-phase (fluid lamellar), at two different values of *RH*: far above the transition (red curves) and directly above the transition (green curves). For each profile, the origin is located at the center of one bilayer, and only one unit cell is shown. Each unit cell contains two half-bilayers plus the water layer floating between them. As illustrated by the schematic drawings at the top of Fig. 5a, b, and c, the low density minima centered at the origin correspond to the lipid terminal methyl group, the adjacent medium-density plateaus correspond to the methylene chain region, and the highest density peaks correspond to the lipid polar headgroups. For all systems investigated the peak position shifted by more than one Å upon hydration. Adjacent to the headgroup peak is the medium-density region associated with the water layer between the bilayers. For the systems studied, the profiles superimpose quite closely from the center towards the edge of the bilayer, indicating that the bilayer structure remains almost unchanged over a wide range of hydration levels. The profiles mainly reflect how the water layer between the bilayers becomes thinner as a result of dehydration, as the headgroup peaks of adjacent bilayers are significantly closer to each other at the low hydration level. EDPs from a series of osmotic stress experiments are shown in the Supplementary Material, Fig. S2 and the corresponding water layer thickness as a function *RH* is shown in the Supplementary Material, Fig. S3. It is found that the d_w-spacing decreases with Chol or PIP_2 concentration.

Next, we have used Eq. (1) to transform the *RH* values into osmotic pressure, in order to plot the osmotic pressure as a function of the water layer thickness d_w, see the example of the PIP_2 presented in Fig. 6. For these plots, the d_w values as obtained from Fig. 4 and analogous curves were used. All measurements are performed in the L-phase where the data points of each sample fall on straight lines in semi-logarithmic

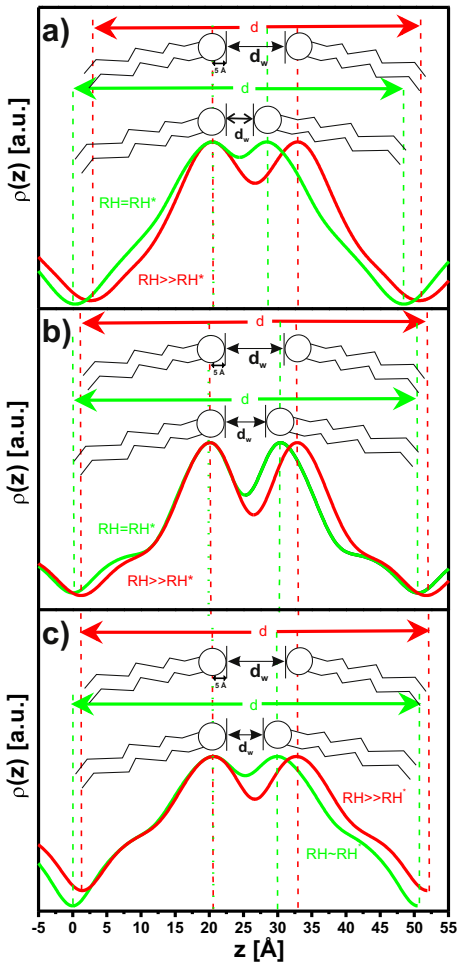

Fig. 5. EDPs for (a) single component lipid (DOPC), (b) binary lipid mixture (DOPC/DOPE: 75/25 mol%), and (c) ternary lipid mixture (DOPC/DOPE/Chol: 52.5/17.5/30 mol%). In each profile just one unit cell is shown where the origin is located at the center of the bilayer. Schematic drawings of the lipid molecules are shown above the profiles, with circles representing the lipid headgroup, and the wavy lines representing L-phase hydrocarbon chains. The EDPs correspond to the L-phase just above the transition level (colored green) and deep in the L-phase (colored red).

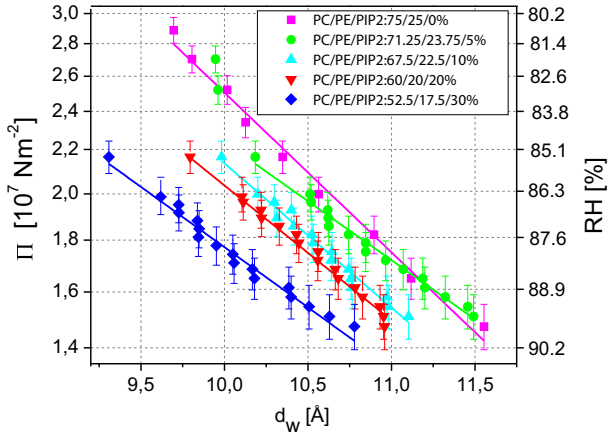

Fig. 6. Plots of natural logarithm of the hydration pressure, Π, vs. water layer, d_w for selected lipid mixtures. The experimental data are extracted from the Eq. (1) with the aid of Fig. 4 along with d_w. The solid lines in each data set are the least-squares fits for each lipid bilayers. In most cases the addition of Chol or PIP_2 facilitates hydration and therefore closes bilayer contact. For all investigated samples, stalk phase formation becomes favorable at $d_w < 9 \pm 0.5$ Å. Lipid molar fraction is indicated in the legend. The solid lines are the least square fits following Eq. (2).

representation, indicating that the osmotic pressure Π decays exponentially with d_w as known from literature [30,13,32,43,46,3]. From the slopes of these lines, we obtain hydration pressure amplitudes as well as the decay constants as given in Table 1. These values can be compared to the previously published values as follows: in single component systems like dipalmitoylphosphatidylcholine (DPPC), egg phosphatidylcholine (EPC), DOPC or DOPE, the values of the decay constant λ_h range $\in$ [1.35, 2.35] Å [32,3], and for binary like mixtures as 1-stearoyl-2oleoyl-phosphatidylcholine/1-palmitoyl-2-oleoyl-phosphatidylethanolamine (SOPC/SOPE), DOPC/DOPE, DOPC or DOPE/Chol and DOPC or DOPE/PIP_2 the values of the decay constant λ_h range $\in$ [2.56, 3.68] Å [43,3]. The ternary mixtures of lipid DOPC/DOPE and Chol or PIP_2 presented here show a similar behavior with the decay constant $\lambda_h \in$ [1.95, 3.29] Å depending on the mixture ratio and contents.

Fig. 7 visualizes the increase of RH^* with Chol or PIP_2 concentration, for constant DOPC/DOPE ratio of 75/25 mol% and 50/50 mol%, respectively. The RH^* values have been directly extracted from reflectivity curves similar to those presented in Fig. 3 and Supplementary Material, Fig. S1. In the following, we discuss the results from a point of view that DOPC/DOPE can be considered as a matrix or majority lipids, and Chol or PIP_2 as additives. Without additive lipids, we know from previous work, that RH^* is considerably higher for 50/50 mol% than for 75/25 mol%. In both cases we observe a further increase with the 'additive' lipid at small concentration followed by a saturation behavior at higher concentration, roughly above 10 mol%. Interestingly, the increase is highest for PIP_2 in the 75/25 mol% matrix, which starts from the lower RH^*. 5 mol% concentration of PIP_2 in this matrix is able to induce an increase in RH^* by more than $\Delta RH^* = 25\%$! Chol also yields a significant, but smaller increase $\Delta RH^* \leq 16\%$ and a roughly equal effect for both matrix concentrations. We find that all mixtures saturate to values bounded by $RH^* \simeq 87\%$, which is the value reached both for PIP_2 in the 75/25 mol% and Chol in the 50/50 mol% matrix, respectively. Hence, we cannot cross the 'barrier' of $RH^* \geq 90\%$, where the osmotic stress method in solution can be used.

To this end, it is of interest to screen for a 'magic' mixture, for which the osmotic pressure needed to induce stalks is small enough, or equivalently RH^* is high enough to cross this 'barrier'. In this structural assay, such a mixture could be considered as extremely fusogenic. Based on small unilamellar vesicle fusion assays, Haque and coworkers have reported "nature's own fusogenic lipid mixture", with the lipid composition DOPC/DOPE/Chol/SM:35/30/15/20 mol% [16], representing a suitable candidate for high RH^*.

Fig. 8a shows a representative XR curve at three distinct regions in the phase diagram of the mixture DOPC/DOPE/Chol/SM:35/30/15/20 mol%: (i) in the lamellar phase (green curve), (ii) at the transition (red curve) where an additional small peak appears, and (iii) below the transition, where two sets of lamellar peaks indicate phase coexistence (blue curve). Thus the mixture exhibits bi-phase behavior at hydration levels below the transition level $RH^* = 90.9\%$, with one phase possibly containing stalks. However, a clear structural analysis is impeded by the phase coexistence. Moreover, due to phase segregation, the concentration of lipids in both phases is not controlled. Fig. 8b shows a comparison between the EDPs of this mixture and others in the L-phase. Adding only Chol into the equimolar DOPC/DOPE 1:1 mixture, slightly reduces the electron density in the headgroup region and increases it in the carbon chain region, but the membrane thickness is approximately the same even at the DOPC/DOPE/Chol:40/40/20 mol%. Contrarily, the bilayer thickens considerably for the 'magic' DOPC/DOPE/

Table 1
The hydration force interaction parameters of DOPC/DOPE and Chol or PIP_2 bilayers at different lipid ratios and degrees of hydration. *RH* denotes the relative humidity in the sample chamber where the least-square fitting is performed; P_0 is the corresponding osmotic pressure coefficient and λ_h is the bilayer hydration interaction constant. The values are extracted from data similar to that presented in Figs. 3 & 4.

Lipid mixture	DOPC/DOPE/Chol				DOPC/DOPE/PIP_2			
Lipid ratio	$P_0[10^9\ J\cdot m^3]$	λ_h [Å]	*RH* [%]	RH^*	$P_0[10^9\ J\cdot m^3]$	λ_h [Å]	*RH* [%]	RH^*
75.0/25.0/0.0	1.14 ± 0.08	2.75 ± 0.04	72.1–89.7	61.3	1.14 ± 0.08	2.75 ± 0.04	82–89.7	61.3
71.3/23.7/5.0	0.94 ± 0.08	2.76 ± 0.06	79.8–92	68.8	0.75 ± 0.18	2.73 ± 0.16	92–89.7	85.3
67.5/22.5/10.0	0.90 ± 0.2	2.86 ± 0.15	72.1–87.5	65.6	0.65 ± 0.10	2.75 ± 0.11	85.3–89.7	86.9
60.0/20.0/20.0	0.86 ± 0.10	2.85 ± 0.09	72.1–85.3	72.1	0.54 ± 0.06	2.86 ± 0.08	85.3–89.7	86.6
52.5/17.5/30.0	0.63 ± 0.06	3.05 ± 0.09	74.3–89.7	72.1	0.29 ± 0.03	3.29 ± 0.12	85.3–89.7	86.3
50.0/50.0/0.0	1.99 ± 0.46	1.95 ± 0.09	82–89.7	71	1.99 ± 0.46	1.95 ± 0.09	82–89.7	71
47.5/47.5/5.0	0.90 ± 0.19	2.43 ± 0.12	85.3–89.7	79.8	0.65 ± 0.09	2.43 ± 0.09	86.4–89.7	79.8
45.0/45.0/10.0	0.35 ± 0.03	2.62 ± 0.06	86.4–92	87.5	0.43 ± 0.07	2.82 ± 0.13	85.3–89.7	79.8
40.0/40.0/20.0	0.45 ± 0.1	2.90 ± 0.19	86.4–89.7	82	0.34 ± 0.12	2.83 ± 0.30	83.1–89.7	79.8
35.0/35.0/30.0	0.34 ± 0.05	3.00 ± 0.13	86.4–89.7	85.3	0.32 ± 0.09	2.84 ± 0.26	86.4–89.7	79.8
Lipid mixture	DOPC/DOPE/DOG: 50/50/x				DOPC/DOG			
DOG fraction	$P_0[10^9\ J\cdot m^3]$	λ_h [Å]	*RH* [%]	RH^*	$P_0[10^9\ J\cdot m^3]$	λ_h [Å]	*RH* [%]	RH^*
0	1.99 ± 0.46	1.95 ± 0.09	71–93.1	71.0	1.50 ± 0.23	2.83 ± 0.11	71–93.1	42.7
1	0.82 ± 0.15	2.35 ± 0.11	79.8–92	75.4	1.42 ± 0.18	2.65 ± 0.09	71–89.7	48.8
5	0.65 ± 0.18	2.57 ± 0.19	79.8–92	77.6	1.22 ± 0.08	2.76 ± 0.05	72.1–92	55.0
10	0.28 ± 0.10	3.32 ± 0.42	79.8–92	78.7	1.28 ± 0.09	2.75 ± 0.05	71–92	56.1
PC/PE/Chol/SM	6.21 ± 0.27	6.00 ± 0.17	84.2–93.1	90.9				

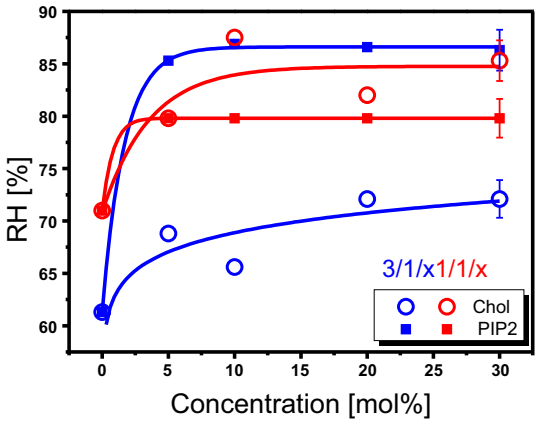

Fig. 7. The transition relative humidity RH^* values were obtained directly from the reflectivity curves (i.e., Fig. 3 & analogous plots). The solid lines correspond to empirical fits which are simply guides to the eye and do not represent any theoretical model. The lipid mixture ratios are indicated on each panel.

Chol/SM:35/30/15/20 mol% mixture, probably caused by an all-trans configuration of the saturated chains of SM. The unusual EDP pin points to the particular nature of this "nature's own fusogenic lipid mixture" [16]. Furthermore, as shown in Fig. 8c, the hydration force is exceptionally small. Fitting of the double logarithmic decay yields $P_0 = 6.2110^7$ J/m^3 and $\lambda = 6.0$ Å, hence values which are very different from all other lipid bilayer mixtures tested, see Fig. 6 and Supplementary Material, Fig. S3. To our knowledge, the decay length $\lambda = 6.0$ is the highest values ever reported. Finally, we have also tested DOG as an additive lipid. The results show that a small molar fraction of DOG also leads to an increase in RH^*, i.e. facilitates the formation of the stalk phase, but bi-phasic or multi-phasic diffraction patterns are observed at DOG concentration higher than 5%, see Supplementary Material, Fig. S5 [51].

5. Discussion and conclusions

In this work we have presented investigations of the phase transition in model lipid membranes, from the fluid lamellar phase (L-phase) to the stalk forming rhombohedral phase (R-phase), extending previous studies [2,3] to lipid ternary and quaternary mixtures. In particular we have investigated how Chol and PIP_2 as important membrane constituents behave in view of the respective propensity for membrane fusion. Starting from pure DOPC bilayers and mixed DOPC/DOPE bilayers, we have increased the respective concentrations and have quantified the shift in the transition point (critical relative humidity (RH^*)) between the L- and the R-phase with Chol and PIP_2 concentration. In this structural assay we qualify a lipid as stalk promoting if it shifts RH^* to higher values, and fusion inhibiting if it shifts RH^* to lower values. While all additive lipids investigated, Chol, PIP_2 and DOG, promote the stalk phase, the respective effects are clearly not additive. For example, DOG has a smaller effect, if a substantial amount of PE as a negative curvature inducing lipid is already present in the 'host'. In other words combining two or three effector lipids, the RH^* increase saturates. It is also found that the additives induce very high shifts in pure DOPC starting at very low $RH^* \simeq 43\%$, but somewhat milder effects, if the RH^* is already quite high such as in DOPC/DOPE. For Chol, the observed effect of stalk promotion may be linked to the known property of Chol to sustain negative curvature [37]. On the other hand, Chol up to 50% concentration is well known as a fluidizing agent by penetrating between the lipid headgroups which also leads to a larger area per headgroup [36]. Also for PIP_2, which has a net negatively charged headgroup, charge repulsion may cause a larger area per lipid [34]. In this sense, one may argue that Chol and PIP_2 have a similar effect on lipid packing.

The present results of how lipid composition affects the L → R transition also illustrate a way in which cellular control of lipid composition

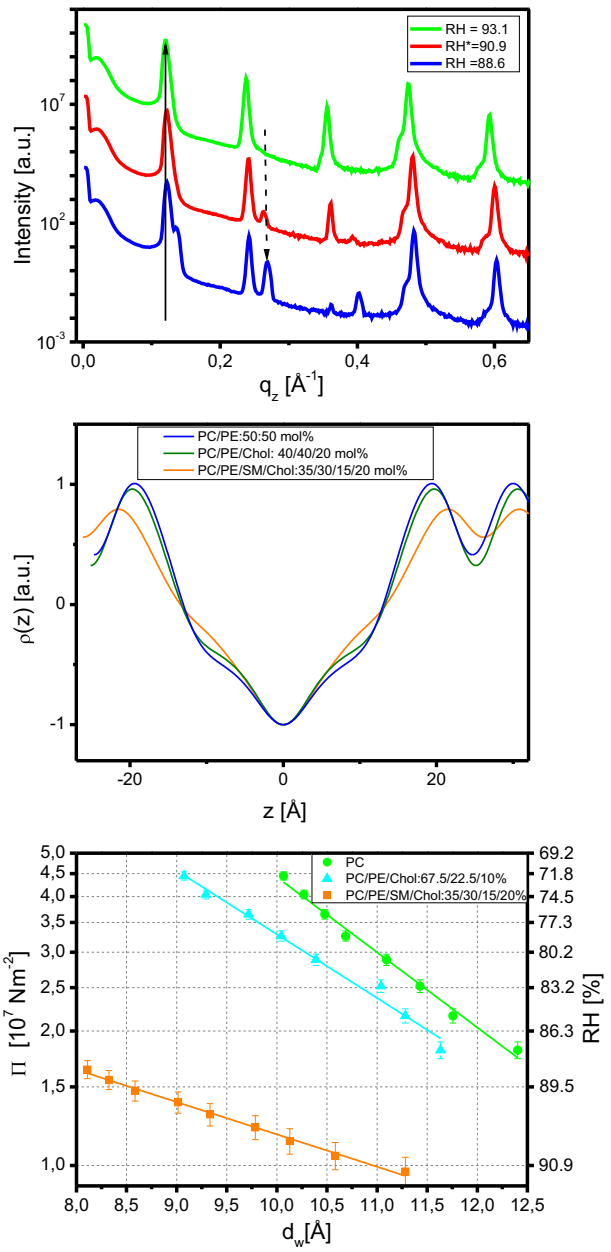

Fig. 8. (a) Representative set of XR curves as a function of the momentum transfer for DOPC/DOPE/SM/Chol: 35/30/15/20 mol% bilayer stacks at various *RH* below and above the transition RH^* level. The curves are shifted vertically for clarity. (b) The EDPs $\rho(z)$ as deduced by the swelling method for various mixtures. The EDPs have been normalized with respect to EDPs in the center of the bilayer, and (c) logarithmic plot of the hydration pressure Π vs. water layer d_w for the mixture DOPC/DOPE/SM/Chol: 35/30/15/20 mol% compared to pure PC and a DOPC/DOPE/Chol mixture.

may provide means to regulate fusion. The increase $\Delta RH^* \simeq 25\%$ upon the addition of Chol or PIP_2 is substantial enough to provide a control mechanism close to the relevant physiologically range, i.e. the local dehydration exerted by fusion proteins, such as in SNARE mediated fusion [21,20], or viral fusion proteins such as the influenza hemagglutinin [7,61,53]. While the fusion proteins set the constraints on the inter-bilayer distance in the context of biological fusion, the constraints are imposed by dehydration in the present study. The rationale behind this is the hypothesis that a fusion protein may locally act in a very similar way as dehydration by osmotic pressure.

In view of the complex mixtures of lipids and proteins encountered in biological fusion, where the composition can be regulated by the cell [47], one may question the validity of the current model system. Such

model systems are necessarily much simpler than the physiologic environment for fusion, containing one or a few lipid species and omitting or simplifying the protein environment. However, both experimental [3] and computational model systems [21] have certainly provided significant insight into the basic physical principles underlying membrane fusion. Furthermore, in designing and interpreting model systems for fusion, it is important to consider how variations in the lipid mixtures chosen may affect the results. One may further raise the argument that local deviations from the average bilayer structure are the decisive factors in fusion, rather than the ensemble average. However the two are clearly interrelated: at certain inter-bilayer distances which are characterized in this work by their ensemble average, individual conformations of lipid become likely to induce fusion, while (local) fusion inducing conformational states of lipids are extremely unlikely at larger separations.

Finally, this work is a first step towards identifying a 'magic' mixture of lipids, which would form the stalk phase also at very mild dehydration, i.e. in a range of osmotic pressures which can also be exerted in excess solvents.

Acknowledgement

We are grateful for the help of Tobias Reusch in bringing the X-ray instrument and humidity control to operation in the initial phase of the project. Financial support by Deutsche Forschungsgemeinschaft (DFG) and Sonderforschungsbereich 803 "Functionality Controlled by Organization in and Between Membranes" is gratefully acknowledged. Z. K. would also like to thank the Hashemite University for the generous support.

Appendix A. Supplementary data

Supplementary data to this article can be found online at http://dx.doi.org/10.1016/j.bbamem.2014.08.010.

References

[1] S. Aeffner, Phospholipids Bilayers: Physical Principles and Models, Universitätsverlag Göttingen, 2012.
[2] S. Aeffner, T. Reusch, B. Weinhausen, T. Salditt, Membrane fusion intermediates and the effect of cholesterol: an in-house X-ray scattering study, EPJE 30 (2009) 205.
[3] S. Aeffner, T. Reusch, B. Weinhausen, T. Salditt, Energetics of stalk intermediates in membrane fusion are controlled by lipid composition, PNAS 109 (2012) E1609–E1618.
[4] G. Basanez, J.L. Nieva, E. Rivas, A. Alonso, F.M. Goni, Diacylglycerol and the promotion of lamellar-hexagonal and lamellar-isotropic phase transitions in lipids: implications for membrane fusion, Biophys. J. 70 (1996) 2299–2306.
[5] A.E. Blaurock, W. Stoeckenius, Structure of the purple membrane, Nature 233 (1971) 152–155.
[6] Z. Chen, R. Rand, The influence of cholesterol on phospholipid membrane curvature and bending elasticity, Biophys. J. 73 (1997) 267–276.
[7] L.V. Chernomordik, V.A. Frolov, E. Leikina, P. Bronk, J. Zimmerberg, The pathway of membrane fusion catalyzed by influenza hemagglutinin: restriction of lipids, hemifusion, and lipidic fusion pore formation, J. Cell Biol. 140 (1998) 1369–1382.
[8] L.V. Chernomordik, M.M. Kozlov, Protein–lipid interplay in fusion and fission of biological membranes*, Annu. Rev. Biochem. 72 (2003) 175–207.
[9] L.V. Chernomordik, M.M. Kozlov, Membrane hemifusion: crossing a chasm in two leaps, Cell 123 (2005) 375–382.
[10] L.V. Chernomordik, M.M. Kozlov, Mechanics of membrane fusion, Nat. Struct. Mol. Biol. 15 (2008) 675–683.
[11] L.V. Chernomordik, G.B. Melikyan, Y.A. Chizmadzhev, Biomembrane fusion: a new concept derived from model studies using two interacting planar lipid bilayers, Biochim. Biophys. Acta Biomembr. 906 (1987) 309–352.
[12] M.A. Churchward, T. Rogasevskaia, J. Höfgen, J. Bau, J.R. Coorssen, Cholesterol facilitates the native mechanism of Ca^{2+}-triggered membrane fusion, J. Cell Sci. 118 (2005) 4833–4848.
[13] S. Das, R.P. Rand, Modification by diacylglycerol of the structure and interaction of various phospholipid bilayer membranes, Biochemistry 25 (1986) 2882–2889.
[14] S.K. Ghosh, S. Aeffner, T. Salditt, Effect of PIP_2 on bilayer structure and phase behavior of DOPC: an X-ray scattering study, ChemPhysChem 12 (2011) 2633–2640.
[15] S.K. Ghosh, S. Castorph, O. Konovalov, R. Jahn, M. Holt, T. Salditt, In vitro study of interaction of synaptic vesicles with lipid membranes, NJP 12 (2010) 105004.
[16] M.E. Haque, T.J. McIntosh, B.R. Lentz, Influence of lipid composition on physical properties and peg-mediated fusion of curved and uncurved model membrane vesicles: nature's own fusogenic lipid bilayer, Biochemistry 40 (2001) 4340–4348.
[17] S.C. Harrison, Viral membrane fusion, Nat. Struct. Mol. Biol. 15 (2008) 690–698.
[18] C. Huang, L. Wheeldon, T. Thompson, The properties of lipid bilayer membranes separating two aqueous phases: formation of a membrane of simple composition, J. Mol. Biol. 8 (1964) 148.
[19] M.B. Jackson, E.R. Chapman, The fusion pores of Ca^{2+}-triggered exocytosis, Nat. Struct. Mol. Biol. 15 (2008) 684–689.
[20] R. Jahn, Some classic papers in the field of membrane fusion—a personal view, Nat. Struct. Mol. Biol. 15 (2008) 655–657.
[21] R. Jahn, H. Grubmueller, Membrane fusion, Curr. Opin. Cell Biol. 14 (2002) 488.
[22] R. Jahn, T. Lang, T.C. Südhof, Membrane fusion, Cell 112 (2003) 519–533.
[23] J. Katsaras, X-ray diffraction studies of oriented lipid bilayers, Biochem. Cell Biol. 73 (1995) 209–218.
[24] S. Kawamoto, W. Shinoda, Free energy analysis along the stalk mechanism of membrane fusion, Soft Matter 10 (2014) 3048–3054.
[25] G. King, C. Worthington, Analytic continuation as a method of phase determination, Phys. Lett. A 35 (1971) 259–260.
[26] M. Kozlov, V. Markin, Possible mechanism of membrane fusion, Biofizika 28 (1983) 242–247 (PDF not found).
[27] B. Lentz, Peg as a tool to gain insight into membrane fusion, Eur. Biophys. J. 36 (2007) 315–326.
[28] B.R. Lentz, M. Hoechli, Y. Barenholz, Acyl chain order and lateral domain formation in mixed phosphatidylcholine–sphingomyelin multilamellar and unilamellar vesicles, Biochemistry 20 (1981) 6803–6809.
[29] C. Li, D. Constantin, T. Salditt, Biomimetic membranes of lipid-peptide model systems prepared on solid support, J. Phys. Condens. Matter 16 (2004) S2439–S2453.
[30] L.J. Lis, V.A. Parsegian, R.P. Rand, Binding of divalent cations to dipalmitoylphosphatidylcholine bilayers and its effect on bilayer interaction, Biochemistry 20 (1981) 1761–1770.
[31] D. Lupyan, M. Mezei, D.E. Logothetis, R. Osman, A molecular dynamics investigation of lipid bilayer perturbation by PIP_2, Biophys. J. 98 (2010) 240–247.
[32] T.J. McIntosh, S.A. Simon, Hydration force and bilayer deformation: a reevaluation, Biochemistry 25 (1986) 4058–4066.
[33] T.J. McIntosh, S.A. Simon, D. Needham, C.H. Huang, Interbilayer interactions between sphingomyelin and sphingomyelin/cholesterol bilayers, Biochemistry 31 (1992) 2020–2024.
[34] S. McLaughlin, D. Murray, Plasma membrane phosphoinositide organization by protein electrostatics, Nature 438 (2005) 605–611.
[35] S. McLaughlin, J. Wang, A. Gambhir, D. Murray, PIP_2 and proteins: interactions, organization, and information flow, Annu. Rev. Biophys. Biomol. Struct. 31 (2002) 151–175.
[36] K. Merz, B. Roux, B. Membranes, A Molecular Perspective From Computation and Experiment, Birkhäuser, Boston, 1996.
[37] O. Mouritsen, M. Zuckermann, What's So Special About Cholesterol?, vol. 39, Springer-Verlag, 2004.
[38] M. Mueller, O. Zschoernig, S. Ohki, K. Arnold, Fusion, leakage and surface hydrophobicity of vesicles containing phosphoinositides: influence of steric and electrostatic effects, J. Membr. Biol. 192 (2003) 33–43.
[39] J. Nagle, D. Wilkinson, Lecithin bilayers. Density measurement and molecular interactions, Biophys. J. 23 (1978) 159–175.
[40] G. Pabst, N. Kucerka, M.-P. Nieh, M. Rheinstädter, J. Katsaras, Applications of neutron and X-ray scattering to the study of biologically relevant model membranes, Chem. Phys. Lipids 163 (2010) 460–479.
[41] S. Raffy, J. Teissié, Control of lipid membrane stability by cholesterol content, Biophys. J. 76 (1999) 2072–2080.
[42] R. Rand, V. Parsegian, Hydration forces between phospholipid bilayers, Biochim. Biophys. Acta Biomembr. 988 (1989) 351–376.
[43] R.P. Rand, N. Fuller, V.A. Parsegian, D.C. Rau, Variation in hydration forces between neutral phospholipid bilayers: evidence for hydration attraction, Biochemistry 27 (1988) 7711–7722.
[44] J. Rizo, C. Rosenmund, Synaptic vesicle fusion, Nat. Struct. Mol. Biol. 15 (2008) 665–674.
[45] T. Salditt, M. Vogel, W. Fenzl, Thermal fluctuations and positional correlations in oriented lipid membranes, PRL 90 (2003) 178101.
[46] E. Schneck, F. Rehfeldt, R.G. Oliveira, C. Gege, B. Demé, M. Tanaka, Modulation of intermembrane interaction and bending rigidity of biomembrane models via carbohydrates investigated by specular and off-specular neutron scattering, Phys. Rev. E. 78 (2008) 061924.
[47] R. Schneiter, B. Brügger, R. Sandhoff, G. Zellnig, A. Leber, M. Lampl, K. Athenstaedt, C. Hrastnik, S. Eder, G. Daum, Electrospray ionization tandem mass spectrometry (ESI-MS/MS) analysis of the lipid molecular species composition of yeast subcellular membranes reveals acyl chain-based sorting/remodeling of distinct molecular species en route to the plasma membrane, J. Cell Biol. 146 (1999) 741–754.
[48] J.M. Seddon, An inverse face-centered cubic phase formed by diacylglycerol–phosphatidylcholine mixtures, Biochemistry 29 (1990) 7997–8002.
[49] D. Siegel, Energetics of intermediates in membrane fusion: comparison of stalk and inverted micellar intermediate mechanisms, Biophys. J. 65 (1993) 2124–2140.
[50] D.P. Siegel, The modified stalk mechanism of lamellar/inverted phase transitions and its implications for membrane fusion, Biophys. J. 76 (1999) 291–313.
[51] D.P. Siegel, J. Banschbach, D. Alford, H. Ellens, L.J. Lis, P.J. Quinn, P.L. Yeagle, J. Bentz, Physiological levels of diacylglycerols in phospholipid membranes induce membrane fusion and stabilize inverted phases, Biochemistry 28 (1989) 3703–3709.
[52] K. Simons, E. Ikonen, Functional rafts in cell membranes, Nature 387 (1997) 569–572.

[53] W. Weissenhorn, A. Hinz, Y. Gaudin, Virus membrane fusion, FEBS Lett. 581 (2007) 2150–2155.
[54] W. Wickner, R. Schekman, Membrane fusion, Nat. Struct. Mol. Biol. 15 (2008) 658–664.
[55] M. Wiener, R. Suter, J. Nagel, Structure of the fully hydrated gel phase of DPPC, Biophys. J. 55 (1989) 315.
[56] M. Wiener, S. White, Fluid bilayer structure determination by the combined use of X-ray and neutron diffraction, Biophys. J. 59 (1991) 162.
[57] X. Xu, E. London, The effect of sterol structure on membrane lipid domains reveals how cholesterol can induce lipid domain formation, Biochemistry 39 (2000) 843–849.
[58] L. Yang, L. Ding, H.W. Huang, New phases of phospholipids and implications to the membrane fusion problem, Biochemistry 42 (2003) 6631–6635.
[59] L. Yang, H.W. Huang, Observation of a membrane fusion intermediate structure, Science 297 (2002) 1877–1879.
[60] L. Yang, H.W. Huang, A rhombohedral phase of lipid containing a membrane fusion intermediate structure, Biophys. J. 84 (2003) 1808–1817.
[61] M.A. Zhukovsky, E. Leikina, I. Markovic, A.L. Bailey, L.V. Chernomordik, Heterogeneity of early intermediates in cell–liposome fusion mediated by influenza hemagglutinin, Biophys. J. 91 (2006) 3349–3358.